On the Foundations of Vision Modelling, IV. Weberized Mumford-Shah Model with Bose-Einstein Photon Noise: Light Adapted Segmentation Inspired by Vision Psychology, Retinal Physiology, and Quantum Statistics

JIANHONG SHEN AND YOON-MO JUNG *

Abstract.

Human vision works equally well in a large dynamic range of light intensities, from only a few photons to typical midday sunlight. Contributing to such remarkable flexibility is a famous law in perceptual (both visual and aural) psychology and psychophysics known as *Weber's Law*. There has been a great deal of efforts in mathematical biology as well to simulate and interpret the law in the cellular and molecular level, and by using linear and nonlinear system modelling tools. In terms of image and vision analysis, it is the first author who has emphasized the significance of Weber's Law in faithfully modelling both human and computer vision, and attempted to integrate it into low level visual processors such as image denoising (*Physica D*, **175**, pp. 241-251, 2003).

The current paper develops a new segmentation model based on the integration of both Weber's Law and the celebrated Mumford-Shah segmentation model (*Comm. Pure Applied Math.*, **42**, pp. 577-685, 1989). Explained in details are issues concerning why the classical Mumford-Shah model lacks light adaptivity, and why its "weberized" version can more faithfully reflect human vision's superior segmentation capability in a variety of illuminance conditions from dawn to dusk. It is also argued that the popular Gaussian noise model is physically inappropriate for the weberization procedure. As a result, the intrinsic thermal noise of photon ensembles is introduced based on Bose and Einstein's distributions in quantum statistics, which turns out to be compatible with weberization both analytically and computationally.

The current paper then focuses on both the theory and computation of the weberized Mumford-Shah model with Bose-Einstein noise. In particular, Ambrosio-Tortorelli's Γ-convergence approximation theory is adapted (*Boll. Un. Mat. Ital.*, **6-B**, pp. 105-123,1992), and stable numerical algorithms are developed for the associated pair of nonlinear Euler-Lagrange PDEs. Numerical results further confirm and highlight the light adaptivity feature of the new model.

Key words. Weber's law, light adaptivity, retina, Mumford-Shah segmentation, Bose-Einstein distribution, noise, Bayesian, variational, free boundary, Γ-convergence, edge wall or well functions, computational PDE.

AMS subject classifications. Primary: 94A08; Secondary: 68U10, 65K10.

> "*Science is built up of facts, as a house is built of stones; but an accumulation of facts is no more a science than a heap of stones is a house.*" -Henri Poincaré

1. Introduction and Motivations. As the title clearly suggests, the current work targets at integrating two facts into the celebrated segmentation model of Mumford and Shah [38]: Weber's Law in vision psychology and retinal physiology, as well as Bose-Einstein statistics for photon ensembles. With Poincaré's words ringing in the air, it is up to the readers to judge whether such effort amounts to a simple accumulation of facts, or otherwise offers at least a new dimension of improvement and

*Shen and Jung are with the School of Mathematics, University of Minnesota, Minneapolis, MN 55455. ({jhshen, ymjung}@math.umn.edu); Tel: (612) 625-3570; Fax: (612) 626-2017. Research is partially supported by (USA) NSF Program in Applied Mathematics under the grant number DMS-0202565.

integration in the "house" building project of human vision modelling.

Light adaptivity is a remarkable feature of human visual perception. During a normal sunshiny midday, entering a relatively dimmer room from outdoor walking, few people ever feel much difference in image interpretation, although physically the average ambient light intensities have undergone a major change. This function has been quantified into a famous law due to Weber [53], and later by Fechner [18], in psychology and psychophysics, whose physiological foundations have also become the focus of many modelling works in mathematical biology [17, 35, 39, 42, 45, 49, 50]. The excellent book by Keener and Sneyd on mathematical physiology [27] has nicely covered this topic as well. Section 2 will give a further detailed account on Weber's Law and its important meaning.

Regretfully, light adaptivity has not drawn much attention from the communities of image processing and vision modelling. It is partially due to the fact that many multimedia image processing tasks only involve *localized still* images, typically like those captured by a digital camera in a fixed environment at a fixed time. Similarly, many application-driven problems such as medical imaging only deal with images with very much *fixed* patterns of intensity distributions, often computed by inverse problem solvers in imaging or signal acquisition technologies.

If one attempts to develop models that emulate more faithfully the superior human visual perception, and implement them inside the machine vision system of a *mobile* robot, then light adaptivity becomes a crucial feature to ensure stable and robust performance for *dynamic* vision.

This claim is well backed up by a familiar phenomenon in photography. It often occurs that an interesting 3-dimensional (3-D) scene looks perfectly fine to the visual perception of a photographer, but appears very dim or weakly contrasted when captured in an analog or digital camera. A camera always faithfully snapshoots the physical luminance of a scene (weather linearly or nonlinearly). It is the human visual perception that has regulated and better conditioned the actually dim scene, and maintained stable perceptual performance.

Thus for the dynamic vision systems of either mobile robots or surveillance cameras, light adaptivity seems a desirable feature to have. In [47], the first author has made the preliminary attempt to introduce it into the total variation based denoising scheme by Rudin, Osher, and Fatemi [44]. In the current work, we take a more systematic and detailed step in integrating light adaptivity (i.e. Weber's Law) into the well known segmentation model of Mumford and Shah [38].

Segmentation is a fundamental task in both machine and human vision. To segment is to partition an image scene Ω into disjoint regions corresponding to individual objects or their fragments, built upon which all vision tasks of higher levels can be further developed using tools from pattern analysis and recognition [24] and the learning theory [41].

In the deterministic (or *cartoonish* [38]) modelling, David Mumford and Jayant Shah formulated the segmentation problem as: given an image observation sample u_0 which might be degraded by noise,

a cartoonish image u and an edge set Γ are to be sought so that on each connected component of $\Omega \setminus \Gamma$, u is smooth or stationary. The solution to segmentation is therefore modelled as an estimation problem, which inevitably falls into the general framework of Bayesian inference [20, 37]:

$$\max_{u,\Gamma} p(u, \Gamma \mid u_0) = \frac{p(u, \Gamma, u_0)}{p(u_0)} = p(\Gamma)p(u \mid \Gamma)p(u_0 \mid u, \Gamma)\frac{1}{p(u_0)}.$$

For the sake of estimation, the probability of the observation $p(u_0)$ is simply a normalization constant and can be set to 1. Then by taking the logarithmic likelihood $E[\cdot] = -\log p(\cdot)$, or formally the "energy" according to Gibbs canonical distribution [21, 37], one arrives at the deterministic segmentation formulation

$$\min_{u,\Gamma} E[u, \Gamma \mid u_0] = E[\Gamma] + E[u \mid \Gamma] + E[u_0 \mid u, \Gamma].$$

Mumford and Shah modelled the three terms by

$$E_{\text{ms}}[u, \Gamma \mid u_0] = \alpha \mathcal{H}^1(\Gamma) + \beta \int_{\Omega \setminus \Gamma} |\nabla u|^2 dxdy + \lambda \int_{\Omega} (u - u_0)^2 dxdy, \tag{1.1}$$

where $\mathcal{H}^1$ stands for 1-D Hausdorff measure, and α, β, and λ are weighting parameters, and will be called *visual potentials* in the present paper [1]. Section 3 gives a further review on the Mumford-Shah model.

The following simple theorem shows that the Mumford-Shah model (1.1) lacks light adaptivity.

THEOREM 1.1 (Gray scale shift-invariance of the Mumford-Shah model). *Suppose that*

$$(u_*, \Gamma_*) = \text{argmin}_{u,\Gamma} E_{\text{ms}}[u, \Gamma \mid u_0]$$

is an optimal estimator of the Mumford-Shah model. Then for any constant gray scale shift θ,

$$(u_* + \theta, \Gamma_*) = \text{argmin}_{u,\Gamma} E_{\text{ms}}[u, \Gamma \mid u_0 + \theta].$$

It immediately implies that an edge can be detected in a dimmer image scene u_0 if and only if when it can be in a brighter scene, say $u_0 + 100$. In particular, for example, a same intensity jump of strength $\delta u_0 = 10$ is perceived with no difference no matter if it is embedded in a dimmer environment of $u_0 \approx 20$ or a brighter one of $u_0 \approx 200$. These conclusions are however inappropriate according to Weber's Law on human visual perception and the principle of light adaptivity.

Following the initial attempt of the first author in [47], the current work intends to introduce light adaptivity into the Mumford-Shah segmentation model (1.1) by incorporating Weber's Law. The new model is called the *weberized Mumford-Shah segmentation model*, where the word "weberization" was first conveniently coined in [47].

[1] Physically, the parameters are like pressure, surface tension, or chemical potentials in statistical mechanics [15, 21].

Furthermore, since weberization necessarily requires to interpret images as light intensity distributions, the shift-invariant Gaussian noise $E[u_0 \mid u, \Gamma]$ in the original Mumford-Shah model becomes physically unjustifiable (though mathematically still a good approximation). For instance, in the Gaussian noise model

$$u_0(x,y) = u(x,y) + n(x,y), \qquad n \text{ subject to the normal distribution } N(0,\sigma^2),$$

the image observation u_0 could become negative, especially in a low-luminance scene when u is small, which is incompatible with Weber's Law where u_0 and u are both light intensities. Therefore, in the current work, by exploring the very physical nature of light, i.e., ensembles of photons subject to Bose-Einstein statistics, we are able to propose a new noise model called *Bose-Einstein noise* which is compatible to weberization.

In summary, the central result of the current work is the proposal of the weberized Mumford-Shah segmentation model with Bose-Einstein noise, which is meaningful in terms of vision psychology, retinal physiology, and the true nature of physics. We shall study both the theoretical and computational aspects of the new model, and compare its performance with that of the classical Mumford-Shah model through both synthetic and real images.

Overall, we wish this piece of work be judged by its rigorous endeavor in developing a more faithful vision model by integrating important experimental and theoretical results in psychology, physiology, and physics, a trend that must be reinforced in the future research of mathematical image and vision analysis (Miva). Moreover, the current work should be best described as targeting at the modelling of the real *human vision* system, rather than merely focusing on digital image processing. In terms of vision modelling, the structure and task of the current work can be depicted by Figure 1.1.

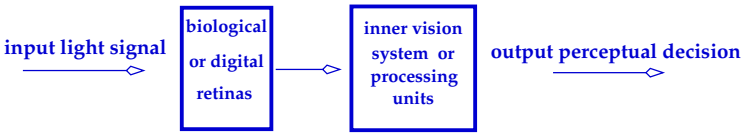

FIG. 1.1. *The current work develops a more faithful model to simulate and interpret human vision's segmentation decisions based on the input light signals or photons striking the two retinas.*

The organization goes as follows. Section 2 reviews the role and essence of Weber's Law in both vision psychology and retinal physiology. Section 3 briefly describes the classical Mumford-Shah model and proves the lack of light adaptivity by analyzing a concrete family of ideal step edges in Theorem 3.1. The weberization procedure is developed in Section 4, together with the development of the physically compatible noise model derived from the Bose-Einstein statistics of photon ensembles. Section 5 then studies the admissible space, the existence theorem (in 1-D case), and the Euler-Lagrange equations of the weberized Mumford-Shah model with Bose-Einstein noise. The techniques employed therein are

very similar to those for the classical model [2, 3, 4, 22, 34, 38]. In Section 6, Ambrosio and Tortorelli's Γ-convergence approximation techniques [3, 4] are adapted to the new model, and a linearization based iterative algorithm is designed for integrating the system of nonlinear Euler-Lagrange equations. The performance of the new model, as well as its comparison with the classical Mumford-Shah model, are finally demonstrated through two examples. Section 7 wraps up the presentation with a brief conclusion.

2. Weber's Law and Light Adaptivity at Retinas. In this section, we introduce the background and roles of Weber's Law in both psychology and physiology.

2.1. Weber's Law in Psychology and Psychophysics. Weber's Law was first qualitatively described by German psychologist E. H. Weber, and later quantified by the great psychologist G. T. Fechner, the father of modern psychophysics.

As an ancient Chinese saying puts it, "In a night with a bright moon, the stars always look scarcer." The fact that human observers are less efficient in spotting the stars in a full-moon night is not caused by the weakened luminance of the stars, rather, the increased luminance of the background sky thanks to the bright moon. Weber's Law characterizes the class of perceptual responses that are more or less parallel to this moon-night phenomenon.

Generally, for both visual and aural perception, let u denote the strength of the mean-field background, and δu the difference or contrast between the background signal and a target signal embedded within. Let $T(\delta u \mid u)$ be the yes-no binary decision of an average human observer for detecting the target signal under a fixed background level u. Then psychological evidences show that $T(\cdot \mid u)$ behaves like a Heaviside function $H(\delta u - \delta_* u)$ for some threshold $\delta_* u$ depending on u:

$$T_u(\delta u \mid u) = H(\delta u - \delta_* u) = 1, \quad \delta u \geq \delta_* u; \quad 0, \quad \text{otherwise.}$$

For each fixed background level u, this threshold $\delta_* u$ is often called the just-noticeable-difference (JND) in psychology. Weber's Law says that the JND is linearly proportional to the mean-field u.

THEOREM 2.1 (Weber's Law). *There exists a constant W, so that for a large range of background mean field u,*

$$\frac{\delta_* u}{u} \equiv W. \tag{2.1}$$

W shall be naturally called Weber's constant or Weber's ratio *in this paper.*

This classical statement of Weber's Law, which is purely empirical, could get further deeper in the eyes of applied mathematicians looking for appropriate perceptual models.

First, the classical statement (2.1) implies that the detection function $T(\delta u \mid u)$ could also be expressed as

$$T(\delta u \mid u) = H\left(\frac{\delta u}{u} - W\right), \tag{2.2}$$

again based on the Heaviside 0-1 function.

In modern quantitative or statistical psychology, decisions are unnecessarily binary. A human subject's responses can lead to a fuzzy inference like "With 62% confidence, the target signal is believed to be embedded in the background field u." Therefore, an ideal perceptual response function shall allow T to be a continuous function that takes any confidence value between 0 and 1. Accordingly the Heaviside function should be replaced by its mollified version.

Such argument reasonably leads to the following empirical theorem.

THEOREM 2.2 (Modified Weber's Law). *Let $T(\delta u \mid u)$ denote the continuous confidence function of perceptual target detection. Then there exists a monotonically increasing function $f(\delta w)$ on $\delta w \in (0, \infty)$, so that $f(0) = 0, f(\infty) = 1$, and $T(\delta u \mid u) = f(\delta u/u)$. Moreover, according to the classical statement of Weber's Law in (2.1), f should bear a sharp transition near Weber constant $\delta w = W$.*

Both statements of Weber's Law overwhelmingly suggest that to human visual or aural perception, the relative contrast $\delta w = \delta u/u$ is a variable more suitable to work with, and can be considered as the net input to the perceptive decision algorithms that human subjects subconsciously employ. This was the primary inspiration that had motivated the earlier work of the first author [47].

An outstandingly enlightening inference from Weber's Law was made by Shapley and Enroth-Cugell [45], and is also highlighted in Keener and Sneyd's book [27].

THEOREM 2.3 (Shapley and Enroth-Cugell's Remarkable Conclusion). *Under Weber's Law, what human vision perceives are the surface material properties of the objects in a visual field, instead of their reflected light.*

First pay attention to the terminologies in the statement. By "perceive," we mean the net effect after being processed by the frontal vision system, instead of the raw light signal striking the two retinas. And by "surface material properties," we mean the geometric (i.e., surface normals) as well as physical (i.e., reflectance indices) properties, both of which are intrinsic to the objects and independent of illuminance.

Thus from Darwin's *Natural Selection* point of view, one can immediately feel the message encoded in Shapley and Enroth-Cugell's clever inference. Vision systems that remain stable and insensitive to illuminance changes are apparently superior to those of the opposite.

Imagine a thunderstorm evening when the eyes of a hungry wolf are locked on its prey (a poor rabbit, say) only ten feet away. If the vision system of the wolf does not function according to Weber's Law or Shapley and Enroth-Cugell's inference, then any lightning flash would very likely deceive the wolf by the illusion that the animal ten feet away is changing. As a result, the wolf could become very confused whether the target is a familiar attackable prey or a new unfamiliar predator. But amid such hesitation, the wolf is lending precious survival time to the rabbit, and could very likely harm itself with a further empty stomach.

In short, it is reasonably likely that Weber's Law results from the *Natural Selection* mechanism.

Proof. (*Quasi-Proof of Shapley and Enroth-Cugell's Inference* [27, 45]) Consider a simple scene only consisting of a background and a target object. Further assume that the background surface as well as the target surface are planar, and the incident light strikes perpendicularly to the two. Let R_B and R_T denote the reflectance indices of the background and the target separately, and I the incident light intensity. Then the reflected light intensities (i.e., observations) u_B and u_T are given by

$$u_B = I \times R_B \quad \text{and} \quad u_T = I \times R_T.$$

According to Weber's Law, the visually perceived difference is given by

$$\frac{|u_B - u_T|}{u_B} = \frac{|IR_B - IR_T|}{IR_B} = \frac{|R_B - R_T|}{R_B},$$

which is indeed independent of the incident light! □

2.2. Weber's Law as Modelled in Mathematical Biology. While psychologically Weber's Law quantitatively describes the perceptual stability with respect to luminance changes, it further raises two related questions:

(a) Why is Weber's Law necessary to human visual perception biologically? and

(b) How is it actually implemented in the visual pathway physiologically? Is it more a "hardware" design in the frontal end (e.g., retinas and ganglion cells [25, 27]) of the vision system, or a "software" implementation in the inner neural networks (e.g., primary visual cortex or V1, etc. [25])?

These are physiological questions underlying Weber's Law, and to no one's surprise, have inspired many modelling works in mathematical biology [17, 35, 39, 42, 45, 49, 50]. James Keener and James Sneyd's remarkable book [27], "*Mathematical Physiology*," gives a very good account of the related literature.

The current theory in mathematical biology believes that Weber's law is realized at the retinal portion of the visual system. More specifically, it is believed to be implemented by the biochemical mechanisms of the photoreceptors, i.e., via various ion channels or pumps across the membranes of rods and cones.

Let I_0 denote the steady background luminance (or light intensity), and $V_0(I_0)$ the corresponding steady membrane potential (of a tagged cone or rod). When I_0 is suddenly increased by an amount of δI to a new level I, the membrane voltage undergoes a transient change $V(t)$:

$$V(0) = V_0(I_0) \quad \text{and} \quad V(t \to \infty) = V_0(I),$$

and in between there is a peak or valley turning point. Let $V(I \mid I_0)$ denote the turning point potential during such a transition, with a possible normalization on the sign and base level. Then $V_0(I_0) = V(I_0 \mid I_0)$.

Based on the response measurement of a red cone of the turtle, Normann and Perlman in 1979 [39] (also reproduced in Keener and Sneyd [27]) obtained a remarkable experimental result that demonstrates a strong pattern well fitted by the Naka-Rushton equation [27]:

$$\frac{V(I|I_0)}{V_{\max}} = \frac{I}{I + A(I_0)}, \tag{2.3}$$

where $V_{\max}$ denotes the saturated and constant potential level, and $A = A(I_0)$ the half-saturation level, so that when $I = A$, $V(I \mid I_0) = V_{\max}/2$. For convenience, we shall normalize the potential so that $V_{\max} = 1$.

Under the condition of *ideal* or *exact* adaptation:

$$V_0(I_0) \equiv const. \qquad \text{independent of the background level } I_0 \geq 0, \tag{2.4}$$

we have

$$const. = V_0(I_0) = V(I_0 \mid I_0) = \frac{I_0}{I_0 + A(I_0)},$$

implying that $A(I_0) = aI_0$ for some constant a. In reality, the ideal adaptation condition is only an approximation, but the experimental result of Normann and Perlman [39] does indicate the slowly varying nature.

Let $\delta I = I - I_0$ denote the contrast change. Then by (2.3) and (2.4), the peak potential response is

$$V(I|I_0) = \frac{I_0 + \delta I}{(a+1)I_0 + \delta I} = \frac{1 + \delta I/I_0}{a + 1 + \delta I/I_0} = f(\delta I/I_0), \quad f(\delta w) = \frac{1 + \delta w}{a + 1 + \delta w}.$$

This well echoes the psychological inference established earlier in Theorem 2.2, and provides a solid physiological way for validating Weber's Law. It again shows the fundamental role of Weber's ratio $\delta w = \delta I/I$ in visual perception.

Define the net peak response by

$$\delta V = \delta V(\delta I \mid I_0) = V(I \mid I_0) - V_0(I_0).$$

Then it is easy to establish

$$\delta V(\delta I \mid I_0) = \frac{a}{(a+1)^2}\frac{\delta I}{I_0} + O((\delta I/I_0)^2).$$

Thus the so called peak sensitivity $S = S(I_0)$ is

$$S(I_0) = \lim_{\delta I \to 0} \frac{\delta V}{\delta I} \propto \frac{1}{I_0},$$

which is another equivalent statement of Weber's Law. Response sensitivity decreases as the background luminance grows stronger, resulting in stable potential responses (i.e., without quick saturation of

membrane potentials by intense bright light), as well as constant performance (i.e., without losing perceptive accuracy in dimmer environments) across a broad range of background luminance levels.

Mathematical modelling efforts in simulating the Weber's Law can be categorized into two classes: algorithmic simulations based on system designs [49, 50], and biochemical simulations based on the dynamics of ions channels and chemical reactions. We again refer to the excellent book by Keener and Sneyd [27] for much details.

3. Mumford-Shah Segmentation Lacks Light Adaptivity.

3.1. A Brief Review of the Mumford-Shah Model. Given an image observation $u_0(x, y)$ on a Lipschitz domain Ω, which in practice is a rectangular domain for most LCD devices, Mumford-Shah's segmentation model [38] is to extract the set Γ of object boundaries from u_0, as well as a cartoonish approximation u on the homogeneous regions $\Omega \setminus \Gamma$, corresponding to the smooth interior of imaged objects.

Such modelling has been motivated by the significance of edges in image understanding and visual perception, as emphasized by David Marr and his colleagues [31, 32] since the very beginning of machine vision research. Embedded within Mumford and Shah's segmentation model is a deterministic image prior – an average image is believed to carry two interdependent components - an edge set Γ, and many homogeneous patches $u\big|_{\Omega_n}$ on the connected components of $\Omega \setminus \Gamma$. Therefore, stochastically speaking, Mumford and Shah's image model belongs to the class of *mixture* models, and is kin to Geman and Geman's earlier mixture model consisting of intensity and line fields [20]. Deterministically, both Mumford-Shah's image and segmentation models lead to *free boundary problems,* which have attracted a great deal of attention from the communities of partial differential equations (PDE), calculus of variations, and geometric measure theory [3, 4, 14, 22, 34].

The mixture image model is specified by a cost functional formally called "energy:"

$$E[u, \Gamma] = E[u \mid \Gamma] + E[\Gamma],$$

where the conditional symbol "|" has been conveniently borrowed from probability theory. The edge regularity energy is measured by

$$E[\Gamma] = \alpha \text{length}(\Gamma), \quad \text{or} \quad \text{the 1-D Hausdorff measure} \quad \alpha \mathcal{H}^1(\Gamma),$$

where α a weighting constant [2]. Conditioning on a given edge set Γ, the "bulk" regularity energy for homogeneous patches is defined by

$$E[u \mid \Gamma] = \beta \int_{\Omega \setminus \Gamma} |\nabla u(x, y)|^2 dx dy,$$

[2] In statistical mechanics, the parameter α corresponds to the surface tension of Γ [15, 21]

implying that the homogeneous patches are modelled as Sobolev functions. As studied in Mumford and Shah's original paper [38], as well as recently re-discovered from the viewpoints of active contouring and level-set implementation by Chan and Vese [14], if β tends to ∞, it becomes necessary that u has zero gradients everywhere away from the edge set. This leads to the reduced Mumford-Shah image model with piecewise constant image priors, or true cartoons.

Finally, Mumford and Shah's *segmentation* model is built upon the mixture image model just developed above, as well as a data model $E[u_0 \mid u, \Gamma]$ that specifies how the image sample u_0 is generated from the target image (u, Γ). Under the general and popular assumption of additive Gaussian white noise:

$$u_0(x, y) = u(x, y) + n(x, y), \quad (x, y) \in \Omega,$$

and its deterministic modification which requires the particular noise sample $n(x, y) \in L^2(\Omega)$, the data model can be naturally generated by the squared error

$$E[u_0 \mid u, \Gamma] = \lambda \int_\Omega (u_0(x, y) - u(x, y))^2 dxdy,$$

where λ is a fitting parameter. By the Bayesian rationale [20, 37], the combination of both the prior image model and data generative model eventually leads to Mumford and Shah's segmentation model:

$$\begin{aligned} \min_{u,\Gamma} E[u, \Gamma \mid u_0] &= E[u, \Gamma] + E[u_0 \mid u, \Gamma] \\ &= E[\Gamma] + E[u \mid \Gamma] + E[u_0 \mid u, \Gamma] \\ &= \alpha \mathcal{H}^1(\Gamma) + \beta \int_{\Omega \setminus \Gamma} |\nabla u|^2 dxdy + \lambda \int_\Omega (u - u_0)^2 dxdy. \end{aligned} \tag{3.1}$$

As far as the minimization task is concerned, the three tunable visual potentials α, β, and λ can be reduced to two by a simple division, or equivalently, setting any one of them to 1.

It turns out that the Mumford-Shah segmentation model is intrinsically connected to a special class of functions with bounded variations, or in short, the space of SBV (Special Bounded Variation). The existence of optimal Mumford-Shah segmentations has been established by De Giorgi, Carriero, and Leaci [22], and Dal Maso, Morel, and Solimini [34], based on the tools for studying SBV [1, 2, 23].

Computational implementations of the Mumford-Shah segmentation model have witnessed three major approaches: (a) the more classical approach based upon finite differences or finite elements [7, 8]; (b) using Osher and Sethian's level-set method [40], as independently developed by Chan and Vese [14], and Tsai, Yezzi, and Willsky [51]; and (c) solving the elliptic PDE's associated with the Γ-convergence approximations of Ambrosio and Tortorelli [3, 4, 29, 30]. For the computation in the current paper, we adopt the Γ-convergence approach.

In addition to its impressive applications in various segmentation tasks, recently the Mumford-Shah image prior model has also been successfully applied the problem of image inpainting [10, 11, 13, 16, 46, 51], as well as extended to incorporate high order geometric features for the sake of faithful inpainting.

By far, the language has been primarily Bayesian, namely, treating the ingredients of the Mumford-Shah segmentation model in terms of prior knowledge and observation generations. On the other hand, in the literature of inverse problems, the Mumford-Shah segmentation model could also be considered as a regularized least square fitting problem, or some sort of Tikhonov regularization technique [48, 52]. Under this view, the three tunable visual potentials are often in the order of

$$\lambda = O(1), \quad \alpha, \beta = o(1) \ll \lambda.$$

3.2. Lack of Light Adaptivity via an Example. In the Mumford-Shah model, the penalty on irregularity is enforced solely based on the measurement of ∇u. The underlying hidden assumption is that the gradients are perceived independent of the background mean fields. But this is inappropriate according to Weber's Law, which claims that light changes are perceived by human vision with an adaptive modulation by the ambient mean fields. Therefore, the effectiveness of the Mumford-Shah segmentation model is at risk in dimmer environments.

Besides Theorem 1.1 in the Introduction section, we now analyze a simple example to further illustrate how the Mumford-Shah segmentation model lacks light adaptivity, as contrast to Weber's Law for human visual perception.

Suppose the image domain $\Omega = \mathbb{R} \times (0, 1)$, and the images to be segmented are a one-parameter family $(u_\delta \mid \delta > 0)$ of *ideal* vertical edges along the y-axis:

$$u_\delta(x, y) = 2\delta + \delta \times (2H(x) - 1) = \delta H(-x) + 3\delta H(x), \tag{3.2}$$

where $H(t)$ denotes the canonical 0-1 Heaviside transition function. The intensity jumps along $\Gamma_0 = \{0\} \times (0, 1)$ are

$$[u_\delta]_{\Gamma_0}(y) = u_\delta(0^+,\ y) - u_\delta(0^-,\ y) \equiv 2\delta.$$

On the other hand, the mean field near the edge is defined by a local averaging

$$\langle u_\delta \rangle = \frac{1}{2A} \int_{(-A,A)\times(0,1)} u_\delta(x, y) dx dy = 2\delta,$$

which is independent of the windowing size A in this ideal setting.

To human visual perception, by Weber's Law, the strength of the edge Γ_0 for any given δ is measured by Weber's ratio:

$$\frac{[u_\delta]}{\langle u_\delta \rangle} = \frac{2\delta}{2\delta} \equiv 1, \quad \text{independent of } \delta\ !$$

Therefore, if it is assumed that Weber's threshold constant W in Theorem 2.1 is less than 1, human perception should always be able to report or detect the existence of the edge Γ_0.

But this is not the case for the machine vision of a robot that implements Mumford-Shah's segmentation model:

$$\min E_{\text{ms}}[u, \Gamma \mid u_\delta] = \alpha \text{length}(\Gamma) + \beta \int_{\Omega \setminus \Gamma} |\nabla u|^2 dxdy + \lambda \int_\Omega (u - u_\delta)^2 dxdy. \tag{3.3}$$

THEOREM 3.1 (Mumford-Shah Model Lacks Light Adaptivity). *For any fixed set of positive visual potentials (α, β, λ), there exists a critical parameter $\delta_c = \delta_c(\alpha, \beta, \lambda)$, such that for any weaker luminance $\delta < \delta_c$,*

$$E_{\text{ms}}[u, \Gamma_0 \mid u_\delta] > \min_v E_{\text{ms}}[v, \phi \mid u_\delta], \tag{3.4}$$

where ϕ denotes an empty edge set, and u any Sobolev output on $\Omega \setminus \Gamma$. That is, if the luminance gets weaker below certain level, the hypothesis of the existence of an edge is not favored in Mumford and Shah's segmentation model.

Proof. First notice that for any desirable segmentation (u, Γ_0),

$$E_{\text{ms}}[u, \Gamma_0 \mid u_\delta] \geq \alpha \text{length}(\Gamma_0) = \alpha.$$

Second, we investigate any compatible segmentation $v = v(x, y)$ that fails to report the presence of the ideal edge Γ_0, for which the Mumford-Shah cost energy is

$$E_{\text{ms}}[v, \phi \mid u_\delta] = \beta \int_\Omega |\nabla v|^2 dxdy + \lambda \int_\Omega (v - u_\delta)^2 dxdy < \infty.$$

By the Schwarz inequality $A + B \geq 2\sqrt{AB}$,

$$\begin{aligned} E_{\text{ms}}[v, \phi \mid u_\delta] &\geq 2\sqrt{\beta\lambda} \int_\Omega |\nabla v| \times |v - u_\delta| dxdy \\ &= \sqrt{\beta\lambda} \left(\int_{\Omega^+} |\nabla (3\delta - v)^2| dxdy + \int_{\Omega^-} |\nabla (v - \delta)^2| dxdy \right), \end{aligned} \tag{3.5}$$

where $\Omega^+ = (0, \infty) \times (0, 1)$ and $\Omega^- = (-\infty, 0) \times (0, 1)$. Notice that the equality holds in the first line if almost surely, $A(x, y) \equiv B(x, y)$. By the vertical translation invariance of both the domain and image u_δ, it can be further assumed that $v = v(x)$ is essentially 1-dimensional and $\nabla = d/dx$. As a result,

$$E_{\text{ms}}[v, \phi \mid u_\delta] \geq \sqrt{\beta\lambda} \left(\int_0^\infty |\nabla (3\delta - v(x))^2| dx + \int_{-\infty}^0 |\nabla (v(x) - \delta)^2| dx \right). \tag{3.6}$$

On the other hand, the compatibility condition also implies that

$$\int_0^\infty (3\delta - v(x))^2 dx < \infty \quad \text{and} \quad \int_{-\infty}^0 (v(x) - \delta)^2 dx < \infty.$$

In particular, there is a sequence of (x_n) so that as $x_n \to +\infty$, $\lim_{n \to +\infty} v(x_n) = 3\delta$. Therefore, according to the definition of total variation,

$$\begin{aligned} \int_0^\infty |\nabla (3\delta - v(x))^2| dx &= \lim_{n \to \infty} \int_0^{x_n} |\nabla (3\delta - v(x))^2| dx \\ &\geq \lim_{n \to \infty} |(3\delta - c)^2 - (3\delta - v(x_n))^2| \\ &= (3\delta - c)^2, \ n \to \infty, \end{aligned}$$

where $c = v(0)$. Notice that equality holds in the second line if $v(x)$ is monotonic.

Similarly, one can show that

$$\int_{-\infty}^{0} |\nabla(v(x) - \delta)^2 dx \geq (c - \delta)^2,$$

and the equality holds if v is monotonic. Hence in combination, (3.6) leads to

$$E_{\rm ms}[v, \phi \mid u_\delta] \geq \sqrt{\beta\lambda}\left((c-\delta)^2 + (3\delta - c)^2\right).$$

Varying $c = v(0)$, one easily sees that the lowest value on the right hand side is obtained when $c = 2\delta = \langle u_\delta \rangle$. Therefore,

$$E_{\rm ms}[v, \phi \mid u_\delta] \geq 2\sqrt{\beta\lambda}\,\delta^2. \tag{3.7}$$

On the other hand, the lower bound in (3.7) is indeed attainable. To see it, define a Sobolev function $v_*(x) \in H^1_{\rm loc}(-\infty, \infty)$ by the following procedure. On $(0, \infty)$, $v_*(x)$ solves the linear initial value problem

$$v_*(0) = 2\delta \quad \text{and} \quad v_*'(x) = \sqrt{\lambda/\beta}\,(3\delta - v_*(x)), \quad x > 0 \tag{3.8}$$

and on $(-\infty, 0)$, $v_*(x)$ solves the backward initial value problem

$$v_*(0) = 2\delta \quad \text{and} \quad v_*'(x) = \sqrt{\lambda/\beta}\,(v_*(x) - \delta), \quad x < 0. \tag{3.9}$$

Then all the equality conditions are indeed met in all the preceding inequalities starting with (3.5). On the other hand, this optimal v_* can be easily solved explicitly:

$$v_*(x) = (3\delta - \delta e^{-\sqrt{\lambda/\beta}\,x})\,H(x) + (\delta + \delta e^{\sqrt{\lambda/\beta}\,x})\,H(-x).$$

Therefore we have proved that

$$\min_v E_{\rm ms}[v, \phi \mid u_\delta] = E_{\rm ms}[v_*, \phi \mid u_\delta] = 2\sqrt{\beta\lambda}\,\delta^2.$$

Finally, define the critical luminance level

$$\delta_c = \delta_c(\alpha, \beta, \lambda) = \sqrt{\frac{\alpha}{2\sqrt{\beta\lambda}}}.$$

Then the inequality (3.4) holds for all $\delta < \delta_c$, which completes the proof. □

4. Weberized Mumford-Shah Model with Bose-Einstein Photon Noise (WMS-BE). In this section, we introduce the main model by incorporating Weber's Law into the Mumford-Shah model. In addition, instead of the popular Gaussian noise model, we introduce a new noise model based on the quantum statistics of photons - the Bose-Einstein statistics, that is compatible to the idea of weberizing the Mumford-Shah model.

4.1. Weberized Mumford-Shah Regularity. To introduce light adaptivity into the classical Mumford-Shah segmentation model, we propose to combine it with Weber's Law through the following procedure.

The gradient at any pixel (x, y) is

$$|\nabla u(x,y)|h \simeq \sqrt{(\delta_{x,h}u(x,y))^2 + (\delta_{y,h}u(x,y))^2},$$

where $h > 0$ denotes the grid size, and

$$\delta_{x,h}u(x,y) = u(x+h,y) - u(x,y) \quad \text{and} \quad \delta_{y,h}u(x,y) = u(x,y+h) - u(x,y)$$

are the contrasts along x and y. In many digital applications, especially numerical computations, h could be treated as fixed.

To apply Weber's Law in a localized setting, one attempts to have the local contrasts $\delta_{x,h}u$ or $\delta_{y,h}u$ modulated by the associated local mean fields. As well practiced in nonlinear image filtering and the theory of scale spaces (see Catté, Lions, Morel, and Coll [6] for example), the local mean field at a pixel (x, y) can be defined through Gaussian smoothing with some window size $\sigma \ll 1$. That is, define

$$G_\sigma(x,y) = \frac{1}{2\pi\sigma^2} \exp\left(-\frac{x^2+y^2}{2\sigma^2}\right),$$

and the local mean field $\langle u \rangle$ at (x, y) to be

$$\langle u \rangle(x,y) = u_\sigma(x,y) = G_\sigma * u(x,y).$$

Here for convenience it has been assumed that the imaging domain $\Omega = \mathbb{R}^2$. For a finite domain, one may run the linear heat equation to the image and terminate the process at a stopping time T that is proportional to σ^2, since it is well known that the essential spreading rate of Brownian motion is $\sqrt{t}$ at any time t. Then according to Weber's Law, the perceptual responses to the luminance contrasts $\delta_{x,h}u(x,y)$ and $\delta_{y,h}u(x,y)$ are

$$\frac{|\delta_{x,h}u(x,y)|}{u_\sigma(x,y)} \quad \text{and} \quad \frac{|\delta_{y,h}u(x,y)|}{u_\sigma(x,y)}.$$

Thus the perceived gradient is

$$\sqrt{\frac{(\delta_{x,h}u)^2}{(u_\sigma)^2} + \frac{(\delta_{y,h}u)^2}{(u_\sigma)^2}} \simeq \frac{|\nabla u|}{u_\sigma}\, h, \quad h \ll 1.$$

As a result, this suggests that as a penalty for irregularities, the bulk cost function $E[u \mid \Gamma]$ in the original Mumford-Shah model should be replaced by the *perceptual* irregularity energy

$$E_{\mathrm{w}}[u \mid \Gamma] = \beta \int_{\Omega\setminus\Gamma} \frac{|\nabla u|^2}{u_\sigma^2}\, dxdy.$$

We call $E_w[u \mid \Gamma]$ the weberized version of $E[u \mid \Gamma]$.

On the other hand, as long as $u \in L^\infty(\Omega \setminus \Gamma)$ (a property that will be justified later), $E_{\rm w}[u \mid \Gamma] < \infty$ requires that u belongs to the Sobolev space $H^1(\Omega \setminus \Gamma)$, making unnecessary the local smoothing procedure $u \to u_\sigma = G_\sigma * u$ for robustly getting the localized mean field $\langle u \rangle$. Thus one could simply take $\langle u \rangle(x,y) = u(x,y)$ at each pixel, and refresh the weberized regularity to

$$E_{\rm w}[u \mid \Gamma] = \beta \int_{\Omega \setminus \Gamma} \frac{|\nabla u|^2}{u^2}\, dxdy. \tag{4.1}$$

For digital implementation with a finite pixel grid size h, however, it may still be a good idea to apply a local smoothing (e.g., 5-point neighborhood averaging) for computing the mean field at each pixel robustly.

4.2. Compatible Noise Model: Bose-Einstein Statistics. Parallel to the weberization of the bulk regularity energy $E[u \mid \Gamma] \to E_{\rm w}[u \mid \Gamma]$, it is also necessary to update the noise model or the fidelity cost function $E[u_0 \mid u]$.

In Weber's Law, the signal u represents light intensity, a nonnegative quantity well defined in both wave and particle mechanics. In particular, for example, $u = 0$ carries the very specific and important physical meaning that there is no single photon or light at all (the *black hole* condition, as called by the first author in [47]). Therefore, the phase space of u is not translation invariant and the associated noise model must show such compatibility.

Due to the *Central Limit Theorem*, Gaussian white noise has been the most popular noise model in the literature of image processing, and so has become the *least square fitting* energy:

$$E_2[u_0 \mid u, \Gamma] = E_2[u_0 \mid u] = \lambda \int_\Omega (u - u_0)^2 dxdy.$$

But what is the physical base for Gaussian becoming a faithful model of optical or photonic noise? Is it because of the universal presence of Brownian motions? Questions like these have seldom been asked in the literature, resulting in the inertial and convenient settling down with the Gaussian white noise.

Many researchers [9, 43, 44] have also studied the multiplicative noise model

$$u_0(x,y) = u(x,y) \times (1 + n(x,y)),$$

with n again modelled by Gaussian or truncated Gaussian (so that $n > -1$ and both u_0 and u could be nonnegative). As a result, the fitting energy becomes [43, 44]

$$E_\times[u_0 \mid u] = \lambda \int_\Omega \left(\frac{u_0}{u} - 1\right)^2 dxdy.$$

But the physical foundations of the multiplicative as well as the Gaussian nature can once again be questioned, and the answers have never come clear in the literature either.

Our approach for an appropriate noise model that is compatible to Weber's Law is based on the very nature of photons, or Bose-Einstein statistics.

By the quantum theory of (free) electromagnetic field, the Hamiltonian can be decomposed into a sum of singleton harmonic oscillators, each of which is identified by a specific base frequency ω_k, $k = 1, 2, \cdots$, or equivalently, quantal energy $\varepsilon_k = \hbar\omega_k$, where $\hbar$ is the Plank constant. The energy spectra of an ε_k-harmonic oscillator, modulated by its ground state $\varepsilon_k/2$, consist of

$$0,\ \varepsilon_k,\ 2\varepsilon_k,\ \cdots,\ n\,\varepsilon_k, \cdots .$$

In terms of the basic photon ε_k, the quantal energy $n\varepsilon_k$ can be interpreted as a group of n particles.

A complete description of a state of the light is therefore specified by the so called *occupation numbers*:

$$\boldsymbol{u} = (u_1,\ u_2,\ \cdots) \in \mathbb{Z}_+^\infty,$$

where $\mathbb{Z}_+$ denotes all nonnegative integers, and each u_k counts the number of ε_k-photons.

Since photons are bosons, each u_k can indeed be any nonnegative integers, as contrast to the fermions (e.g., electrons), for which u_k can only be either 1 or 0, representing the on-off states of being occupied or not [15, 21].

At thermal equilibrium with a fixed temperature T, an ensemble of photons obey the Bose-Einstein statistics. That is, for any state $\boldsymbol{u}$ with total energy

$$E[\boldsymbol{u}] = \sum_{k=1}^{\infty} u_k\varepsilon_k = \hbar\sum_{k=1}^{\infty} u_k\omega_k,$$

the Bose-Einstein probability $p(\boldsymbol{u})$ is analogous to Gibbs' canonical ensemble:

$$p(\boldsymbol{u}) = \frac{1}{Z_\beta}\exp(-\beta E[\boldsymbol{u}]),$$

where $\beta = 1/(kT)$ is the inverse temperature normalized by the Boltzmann constant k. Therefore the partition function is given by

$$\begin{aligned} Z_\beta &= \sum_{\boldsymbol{u}\in\mathbb{Z}_+^\infty} \exp(-\beta E[\boldsymbol{u}]) = \sum_{\boldsymbol{u}\in\mathbb{Z}_+^\infty}\prod_{k=1}^{\infty}\exp(-\beta\varepsilon_k u_k) \\ &= \prod_{k=1}^{\infty}\sum_{u_k=0}^{\infty}\exp(-\beta\varepsilon_k u_k) = \prod_{k=1}^{\infty}\frac{1}{1-e^{-\beta\varepsilon_k}}. \end{aligned} \tag{4.2}$$

Hence, for any ε_k-species of photons, the average occupation number is

$$\langle u_k\rangle = \frac{\partial(-\ln Z_\beta)}{\partial(\beta\varepsilon_k)} = \frac{1}{e^{\beta\varepsilon_k}-1}, \quad k = 1, 2, \cdots . \tag{4.3}$$

As a simplified model, let us now consider monochromatic light or an ensemble of photons of a same species with quantal frequency ω_0 and energy $\varepsilon_0 = \hbar\omega_0$. Let u_0 denote the observed number of photons each time, and $u = \langle u_0 \rangle$ its mean.

At thermal equilibrium with temperature T, the Bose-Einstein distribution becomes

$$p(u_0) = \frac{1}{Z_\beta} \exp(-\beta\varepsilon_0 u_0) = \frac{1}{Z_\beta} \exp\left(-\frac{\varepsilon_0 u_0}{kT}\right), \quad u_0 = 0, 1, \cdots.$$

And the partition function and the average number are

$$Z_\beta = \frac{1}{1 - e^{-\beta\varepsilon_0}} \qquad \text{and} \qquad u = \langle u_0 \rangle = \frac{1}{e^{\beta\varepsilon_0} - 1}. \tag{4.4}$$

Therefore,

$$e^{-\beta\varepsilon_0} = \frac{u}{1+u} \quad \text{and} \quad Z_\beta = \left(1 - \frac{u}{1+u}\right)^{-1} = 1 + u.$$

When the light is not too weak so that the mean number of photons $u \gg 1$, one has $\beta\varepsilon_0 \ll 1$ and

$$u \simeq \frac{1}{\beta\varepsilon_0} \quad \text{and} \quad p(u_0) = p(u_0 \mid u) \simeq \frac{1}{u} \exp\left(-\frac{u_0}{u}\right).$$

In particular, in the continuum limit, one can assume that $u_0 \in (0, \infty)$, and the above is precisely the exponential distribution with average observation u.

Therefore, the logarithmic likelihood function is given by

$$e(u_0 \mid u) = -\ln p(u_0 \mid u) = \ln u + \frac{u_0}{u}.$$

For a given imaging plane or lattice Ω, the sum of this likelihood function over the entire domain (assuming free photons without spatial interactions) yields the new fidelity energy

$$E_{\text{be}}[u_0 \mid u] = \lambda \int_\Omega e(u_0(x,y) \mid u(x,y)) dxdy = \lambda \int_\Omega \left(\ln u(x,y) + \frac{u_0(x,y)}{u(x,y)}\right) dxdy, \tag{4.5}$$

which is different from the popular Gaussian or least square models either additive or multiplicative. We shall call it the Bose-Einstein noise model.

Notice that the form of $e(u_0 \mid u)$ does require the purity of the photon species at a target sensor. However across the entire imaging plane or domain Ω, the independent summation in E_{be} does not demand a spatial uniformity of the species. That is, near two distinct sensors A and B, the photon species can be ω_A and ω_B with $\omega_A \neq \omega_B$, which makes E_{be} more plausible in approximating real situations. Notice that in the wave theory of light, all the above can be similarly explained via the stationary phase method in asymptotic analysis (see, e.g., [5]).

Finally, away from both physics and statistics, one can simply accept E_{be} in (4.5) as a new form of fitting cost, polishing the popular least square error. Such viewpoint is especially helpful in the Tikhonov framework for image restoration and segmentation [52, 48].

4.3. The Model: Weberized Mumford-Shah with Bose-Einstein Noise. In combination of the preceding two subsections, we thereby propose the following weberized Mumford-Shah model with Bose-Einstein noise:

$$\begin{aligned} E_{\text{wmsbe}}[u, \Gamma \mid u_0] &= E[\Gamma] + E_{\text{w}}[u \mid \Gamma] + E_{\text{be}}[u_0 \mid u] \\ &= \alpha \mathcal{H}^1(\Gamma) + \beta \int_{\Omega \setminus \Gamma} \frac{|\nabla u|^2}{u^2} dxdy + \lambda \int_{\Omega} \left(\ln u + \frac{u_0}{u} \right) dxdy. \end{aligned} \tag{4.6}$$

Unlike the classical Mumford-Shah model, here the images u and u_0 are both understood as light intensity distributions as in Weber's Law, or equivalently, both count the number of photons. In particular, we must have

$$u(x, y), \quad u_0(x, y) > 0, \quad \text{on} \quad \Omega.$$

Or more conveniently, define the logarithmic intensities

$$w(x, y) = \ln u(x, y) \quad \text{and} \quad w_0(x, y) = \ln u_0(x, y).$$

Then the weberized Mumford-Shah energy naturally applies to w and w_0:

$$\begin{aligned} E_{\text{wmsbe}}[w, \Gamma \mid w_0] &= E[\Gamma] + E_{\text{w}}[w \mid \Gamma] + E_{\text{be}}[w_0 \mid w] \\ &= \alpha \mathcal{H}^1(\Gamma) + \beta \int_{\Omega \setminus \Gamma} |\nabla w|^2 dxdy + \lambda \int_{\Omega} \left(w + e^{w_0 - w} \right) dxdy. \end{aligned} \tag{4.7}$$

Notice that w and w_0 can now both take negative values. In fact the last model (4.7) looks more similar to the original Mumford-Shah model except for the noise model and the logarithmic transform.

We have thus successfully completed the modelling stage, and the rest of the paper will focus on the analysis and computation of the model (4.6) or (4.7), which cannot impose too brand new challenges due to the similarity between the transformed model (4.7) and the classical Mumford-Shah model. In particular, one can profoundly benefit from the rich existing literature on the Mumford-Shah model [2, 3, 4, 34, 22].

5. Study of the WMS-BE Model.

5.1. Admissible Spaces. From the last term on Bose-Einstein noise in the new model (4.7), it is natural to assume that $w(x, y) \in L^1(\Omega)$. On the other hand, as in the classical Mumford-Shah model, the first two terms on the logarithmic prior suggest that w belongs to $\text{SBV}(\Omega)$, the special functions of bounded variations:

$$Dw = \nabla w + [w] \times \mathcal{H}^1 \big|_{\Gamma},$$

where Dw denotes the vectorial Radon measure associated with the distributional derivative of w, ∇w the Lebesgue continuous part (or the Sobolev component), and $[w]$ the jump along the oriented jump set $\Gamma = \Gamma_w$, which is well defined almost surely according to the 1-D Hausdorff measure.

The logarithmic transform of the noise model also requires

$$e^{w_0(x,y)-w(x,y)} \in L^1(\Omega).$$

By the principle of L^p duality, it is therefore natural (pragmatic, convenient, but not necessarily unique) to assume that

$$e^{w_0} \in L^\infty(\Omega) \quad \text{and} \quad e^w \in L^1(\Omega).$$

Consequently, $w_0 \in L^\infty(\Omega)$. The next theorem shows that one can simply demand $w \in L^\infty(\Omega)$ as a result.

THEOREM 5.1. *Let $w_*(x,y)$ be a minimizer to the weberized Mumford-Shah model $E_{\text{wmsbe}}[w, \Gamma \mid w_0]$ (4.7) with Bose-Einstein noise. Assume that the logarithmic light intensity observation $w_0 \in L^\infty(\Omega)$. Then $w_* \in L^\infty(\Omega)$ and $\|w_*\|_\infty \le \|w_0\|_\infty$.*

Proof. For any real parameter a, define a nonlinear function by

$$\psi(t \mid a) = t + e^{a-t}, \quad t \in \mathbb{R}. \qquad \text{Then,}$$

$$\psi'(t \mid a) = 1 - e^{a-t} \quad \text{and} \quad \psi''(t \mid a) = e^{a-t}.$$

In particular, $\psi(\cdot \mid a)$ is strictly convex for any fixed a. Since $\psi(\pm\infty) = +\infty$, and $\psi'(a \mid a) = 0$, we conclude that $t_* = a$ is the unique minimizer of $\psi(\cdot \mid a)$ for any a. As a result, for any t_1, t_2 with

$$(t_1 - a)(t_2 - a) \ge 0 \quad \text{and} \quad |t_1 - a| \le |t_2 - a|,$$

one has $\psi(t_1 \mid a) \le \psi(t_2 \mid a)$ and the inequality holds if and only if $t_1 = t_2$.

Now assume $\|w_0\|_\infty = A$ and define the truncated function from the minimizer w_* by

$$[w_*]_A(x,y) = w_*(x,y) \times \left(1 \wedge \frac{A}{|w_*(x,y)|}\right), \quad (x,y) \in \Omega.$$

Following the preceding preparation, at any pixel (x,y), identifying

$$a = w_0(x,y), \quad t_1 = [w_*]_A(x,y), \quad \text{and} \quad t_2 = w_*(x,y),$$

one arrives at

$$\psi([w_*]_A(x,y) \mid w_0(x,y)) \le \psi(w_*(x,y) \mid w_0(x,y)),$$

as well as

$$\int_\Omega \psi([w_*]_A(x,y) \mid w_0(x,y))dxdy \le \int_\Omega \psi(w_*(x,y) \mid w_0(x,y))dxdy. \tag{5.1}$$

The equality in the last equation holds if and only if *a.e.*,

$$[w_*]_A(x,y) = w_*(x,y), \quad \text{or equivalently,} \quad \|w_*\|_\infty \le A \ \ (= \|w_0\|_\infty).$$

On the other hand, according to [4, 22], it is sufficient to work with $w_* \in C^1(\Omega \setminus \Gamma)$. In particular, one can further assume that A is a *regular* value of w_*, meaning that the level sets $w_* \equiv \pm A$ are 1-D manifolds. (Otherwise simply replace A by some $A+\varepsilon$ with $|\varepsilon| \to 0$. This is guaranteed by the denseness and openness of regular values in differential topology [36].) Then, as a Radon measure on $\Omega \setminus \Gamma$ (whose notation will be omitted in the next two lines for simplicity), one has

$$\begin{aligned} D[w_*]_A &= D[w_*]_A\big|_{\{|w_*|<A\}} + D[w_*]_A\big|_{\{|w_*|>A\}} + D[w_*]_A\big|_{\{|w_*|=A\}} \\ &= \nabla w_*\big|_{\{|w_*|<A\}}. \end{aligned}$$

The second term vanishes since $[w_*]_A$ is constant on the open set $|w_*| > A$, while the last term vanishes because w_*, and therefore $[w_*]_A$, are continuous along the 1-D manifolds $|w_*| = A$ (see, e.g., [23]). Remind that here all terms are restricted on $\Omega \setminus \Gamma$. Therefore,

$$\int_{\Omega\setminus\Gamma} |\nabla [w_*]_A|^2 dxdy \le \int_{\Omega\setminus\Gamma} |\nabla w_*|^2 dxdy. \tag{5.2}$$

In combination of (5.1) and (5.2), one arrives at

$$E[\,[w_*]_A, \Gamma \mid w_0] \le E[w_*, \Gamma \mid w_0].$$

Since w_* is a minimizer, the equality must hold. Then the theorem directly follows from the equality condition of (5.1). □

Notice that in the proof one could circumvent the C^1 characterization of [22] by turning to the continuity of the truncation operator $[\cdot]_A$ (both weak and *a.s.*), mollification approximations of $H^1(\Omega \setminus \Gamma)$, and the weak lower semi-continuity properties of Sobolev norms [28]. On the other hand, the proof also clearly demonstrates the good behavior of the Bose-Einstein noise for mathematical analysis.

5.2. Existence Theorem. The remarkable works [2, 3, 4, 22, 34] on the existence of solutions to the classical Mumford-Shah segmentation can be naturally adapted to the weberized Mumford-Shah model with Bose-Einstein noise. For completeness, in what follows, we prove the existence of E_{wmsbe} in the 1-D case. After some necessary adaptation being made, the techniques are nothing very different from the existing literature. For much more involved high dimensional cases, we refer to the aforementioned works in the classical literature.

We assume that the image domain is the unit interval $I = (0,1)$, and denote by Γ_u or equivalently Γ_w the jump set of an admissible image u on I.

THEOREM 5.2 (Existence of Optimal Segmentation by WMS-BE). *Suppose* $w_0 = \ln u_0 \in L^\infty(I)$. *Define* $w = \ln u$, *and*

$$\mathcal{D} = \{u(x) \ : \ \|w\|_\infty \le \|w_0\|_\infty, \ \#\Gamma_w < \infty, \ w \in H^1(I \setminus \Gamma_w)\}.$$

Then the minimizer in $\mathcal{D}$ exists to the weberized Mumford-Shah model with Bose-Einstein noise:

$$E_{\text{wmsbe}}[u, \Gamma \mid u_0] = \alpha \#\Gamma + \beta \int_{I \setminus \Gamma} \frac{|\nabla u|^2}{u^2} dx + \lambda \int_I \left(\ln u + \frac{u_0}{u} \right) dx,$$

or equivalently, its logarithmic version $E_{\text{wmsbe}}[w, \Gamma \mid w_0]$.

Notice that the restriction $\|w\|_\infty \leq \|w_0\|_\infty$ has been well justified by Theorem 5.1.

Proof.

(a) First notice that $E_{\text{wmsbe}}[w, \phi \mid w_0] < \infty$ for $w \equiv 0 \in \mathcal{D}$. Thus one can assume that there is a (logarithmic) minimizing sequence $\{w_n\}_{n=1}^\infty \subset \mathcal{D}$ whose E_{wmsbe} energies are bounded by some finite value, say, M.

(b) Let Γ_n denote the associated jump set of w_n. Then $\{\#\Gamma_n\}$ is uniformly bounded. With a possible subsequence refinement, one could assume that $\#\Gamma_n \equiv N$ for $n = 1, 2, \cdots$, and that

$$\Gamma_n = \{x_1^{(n)} < x_2^{(n)} < \cdots < x_N^{(n)}\} \subset I.$$

By the pre-compactness of bounded sequences in $\mathbb{R}$, with possibly another round of subsequence refinement, one could assume that there exists a limiting set (possibly a multiset)

$$\Gamma^* = \{x_1^* \leq x_2^* \leq \cdots \leq x_N^*\} \subset \bar{I} = [0, 1],$$

and for each $j = 1 : N$, $x_j^{(n)} \to x_j^*$ as $n \to \infty$.

(c) For any $\varepsilon > 0$, define the (relatively) closed ε-neighborhood of Γ^* in $I = (0, 1)$ by

$$\Gamma_\varepsilon^* = \{y \in I \ : \ \text{dist}(y, \Gamma^*) \leq \varepsilon\},$$

and its open complement $I_\varepsilon = I \subset \Gamma_\varepsilon^*$. Then as $\varepsilon \to 0$, I_ε monotonically expands to I. For any fixed ε, there exists an n_ε, so that for any $n > n_\varepsilon$, w_n's are bounded in $H^1(I_\varepsilon)$ since

$$\|w_n\|_{H^1(I_\varepsilon)}^2 = \int_{I_\varepsilon} w_n^2(x) dx + \int_{I_\varepsilon} (w_n'(x))^2 dx \leq \|w_0\|_\infty^2 + \frac{M}{\beta},$$

as long as Γ_n starts to be included within Γ_ε^*.

(d) Choose any sequence (ε_k) with $\varepsilon_k \to 0$ as $k \to \infty$. For ε_1, by the compactness of $H^1(I_{\varepsilon_1})$ in $L^2(I_{\varepsilon_1})$ [33], one could refine a subsequence of $(n)_{n=1}^\infty$, denoted by $(n \mid 1)_{n=1}^\infty$, so that $(w_{(n|1)})_{n=1}^\infty$ is a Cauchy sequence in $L^2(I_{\varepsilon_1})$.

Repeating this process, for each step $k \geq 2$, one could find a subsequence $(n|k)$ of $(n|k-1)$ so that $(w_{(n|k)})_{n=1}^\infty$ is a Cauchy sequence in $L^2(I_{\varepsilon_k})$. Finally, define $w_k^* = w_{(k|k)}$, $k = 1 : \infty$.

(e) Then it is clear there that there exists a unique $w^* \in L^2_{\text{loc}}(I \setminus \Gamma^*)$, so that $w_k^* \to w^*$ in any $L^2(I_\varepsilon)$. In particular,

$$\|w^*\|_\infty \leq \|w_0\|_\infty.$$

Furthermore, by the L^2 lower semi-continuity of Sobolev norms, on any I_ε,

$$\int_{I\setminus\Gamma^*} |(w^*)'|^2 dx = \sup_\varepsilon \int_{I_\varepsilon} |(w^*)'|^2 dx \le \sup_\varepsilon \liminf_{k\to\infty} \int_{I_\varepsilon} |(w_k^*)'|^2 dx \le \liminf_{k\to\infty} \int_{I\setminus\Gamma_{(k|k)}} |(w_k^*)'|^2 dx.$$

Since (w_k^*) is a minimizing sequence, we conclude that $w^* \in H^1(I\setminus\Gamma^*)$, $\Gamma_{w^*} \subset \Gamma^*$, and $w^* \in \mathcal{D}$.

(f) With a possible subsequence refinement, one could assume

$$w_k^*(x) \to w^*(x), \quad a.e. \quad x \in I.$$

Following the notation in the proof of Theorem 5.1, we then must have

$$\psi(w_k^*(x) \mid w_0(x)) \to \psi(w^*(x) \mid w_0(x)) \quad a.e. \quad x \in I,$$

as a result of the continuity of $\psi(t \mid a)$. Since w_0 and all w_k^*'s are bounded by $A = \|w_0\|_\infty$, so is ψ's by

$$|\psi(w_k^*(x) \mid w_0(x))| \le A + e^{2A}, \quad \forall k, x.$$

Then, by *Lebesgue's Dominated Convergence Theorem*,

$$\int_I \psi(w^* \mid w_0) dx = \lim_{k\to\infty} \int_I \psi(w_k^* \mid w_0) dx.$$

(g) In combination of the last two itemized results, we arrives at

$$E_{\text{wmsbe}}[w^*, \Gamma_{w^*} \mid w_0] \le \liminf_{k\to\infty} E_{\text{wmsbe}}[w_k^*, \Gamma_{w_k^*} \mid w_0].$$

Since (w_k^*) is a minimizing sequence, $w^* \in \mathcal{D}$ has to be a minimizer, which concludes the proof.

□

5.3. Euler-Lagrange Equations. To derive the Euler-Lagrange equations, one defines two *conditional* cost functions associated with E_{wmsbe}, similar to the classical literature.

For a given jump set Γ, define the conditional bulk energy of w to be

$$E[w \mid \Gamma, w_0] = \int_{\Omega\setminus\Gamma} B(w, \nabla w \mid w_0) dxdy, \tag{5.3}$$

where the bulk function

$$B = B(w, \nabla w \mid w_0) = \beta|\nabla w|^2 + \lambda(w + e^{w_0 - w}).$$

Let $w_\Gamma = \text{argmin} E[w \mid \Gamma, w_0]$ be the minimizer for the given jump set Γ, which is unique due to the strict convexity. Then $w_\Gamma \in H^1(\Omega\setminus\Gamma)$ must solve the following Euler-Lagrange equation in the distributional sense

$$0 = \frac{\partial B}{\partial w} - \nabla \cdot \left(\frac{\partial B}{\partial \nabla w}\right) = -2\beta\Delta w + \lambda\left(1 - e^{w_0 - w}\right), \tag{5.4}$$

on each connected components Ω_i of $\Omega \setminus \Gamma$, with Neumann adiabatic boundary condition $\partial w/\partial \vec{n} = 0$. Notice that $\partial\Omega_i \subset \partial\Omega \cup \Gamma$.

Next, for the current estimation $w = w_\Gamma$, to compute the variational effect caused by the perturbation of Γ, define the conditional energy

$$E[\Gamma \mid w, w_0] = E[\Gamma \mid B] = \alpha \mathcal{H}^1(\Gamma) + \int_{\Omega\setminus\Gamma} B(w, \nabla w \mid w_0) dxdy.$$

Assuming that Γ is piecewise C^1, near any regular point $\boldsymbol{x}(s) \in \Gamma$ parameterized by the arc length s, a perturbation $\Gamma \to \Gamma_\varepsilon$ can be locally expressed by

$$\boldsymbol{x}(s) \to \boldsymbol{x}_\varepsilon(s) = \boldsymbol{x}(s) + \varepsilon(s) N(s), \qquad |\varepsilon(s)| \ll 1,$$

where $N(s)$ is unit normal at $\boldsymbol{x}(s)$. Adapted to the perturbation of $\Gamma \to \Gamma_\varepsilon$ is the local necessary extension of the bulk function $B(x, y) = B(w, \nabla w \mid w_0) \to B^\varepsilon(x, y)$. Locally according to the orientation of N, the region is segmented by Γ into the tail half and the head half, labelled by "$-$" and "$+$" separately. Accordingly, B is segmented into $B_\pm$ components on each half. Following the perturbation of $\Gamma \to \Gamma_\varepsilon$, locally, B_σ with $\sigma(s) = -\text{sign}(\varepsilon(s))$ can be extended onto the new stripe territory by

$$B^\varepsilon_\sigma(\boldsymbol{x}(s) + tN(s)) = B_\sigma(\boldsymbol{x}(s)), \quad t \in [0, \varepsilon(s)).$$

The conditional energy $E[\Gamma \mid B]$ is naturally perturbed to $E[\Gamma_\varepsilon \mid B^\varepsilon]$, and the standard calculation then gives rise to

$$\delta E = E[\Gamma_\varepsilon \mid B^\varepsilon] - E[\Gamma \mid B] = (-\alpha\kappa N - [B]N) \cdot (\varepsilon N) + O(\varepsilon^2), \tag{5.5}$$

where $[B] = [B](s) = B_+(s) - B_-(s)$ denotes the jump across Γ, and κ the signed curvature, both coupled with N so that although N can have binary uncertainty, both κN and $[B]N$ are unique (and κN points to the center of curvature). Therefore, if (w, Γ) is a minimizer, the jump curve must satisfy

$$\alpha\kappa + [B(w, \nabla w \mid w_0)] = 0.$$

For the sake of numerical computation, as done in Chan and Vese [14], the variational formula (5.5) offers a strategy for local interface motion that is similar to the active contour technique [26]:

$$\frac{\partial \boldsymbol{x}(s,t)}{\partial t} = \alpha\kappa N + [B]N. \tag{5.6}$$

To the jump set or interface, this is a combination of two motion mechanisms: the mean curvature motion that is curve shortening, geometric, and intrinsic, and the motion driven by an external bulk energy B.

The free boundary nature of the Mumford-Shah model makes the computation highly nontrivial. There are many remarkable works on effective implementations of the model, including the finite element

or finite difference methods [7, 8], the level-set method of Osher and Sethian [14, 40, 51], and the Γ-convergence elliptic approximations first proposed by Ambrosio and Tortorelli [3, 4]. In what follows, for the weberized Mumford-Shah model with Bose-Einstein noise, we adopt the approach of Γ-convergence approximations and explore the corresponding computational issues.

6. Γ-Convergence Approximation and Numerical Computation.

6.1. Γ-Convergence Approximation of Ambrosio and Tortorelli. In this section, we adapt Ambrosio and Tortorelli's Γ-convergence approximation scheme in [4] to the new model.

For Γ-convergence approximation, the edge set Γ is encoded by the so called *auxiliary* function $z = z(x, y)$, or the *well* function, which is close to 1 almost everywhere except near the edge set, where it sharply drops to zero or close. Thus, Γ looks like an elongated well or canyon if z is understood as the height field of a territory. The rate as well as the amount of dropping along the edge set are controlled by an approximation parameter $\varepsilon \to 0$. Hence z depends on ε: $z = z_\varepsilon(x, y)$.

The length cost $E[\Gamma] = \alpha \mathcal{H}^1(\Gamma)$ is now replaced by its approximation

$$E_\varepsilon[z] = \alpha \int_\Omega \left(\varepsilon |\nabla z|^2 + \frac{(z-1)^2}{4\varepsilon} \right) dxdy. \tag{6.1}$$

To see approximately why this quadratic functional yields good approximation to the length, consider the following computation in the 1-D case when $\Omega = (-1, 1)$ and $x = 0$ is the only jump point: by the Schwarz inequality $A + B \geq 2\sqrt{AB}$,

$$E_\varepsilon[z] \geq \alpha \int_\Omega |\nabla z||z-1| dx = \frac{\alpha}{2} \int_\Omega |\nabla s(x)| dx, \tag{6.2}$$

where $s = (z-1)^2$ is called the *wall* function (as compared to the calling of z the *well* function). Suppose z indeed behaves like what has been described in the beginning, i.e., ideally $z \simeq 1$ almost everywhere except for near $x = 0$ where it drops to $z(0) \simeq 0$. Then s vanishes almost everywhere except $s(0) \simeq 1$, the top of the "wall." Now that the integral on the right hand side is precisely the total variation of s, and therefore must be approximately 2 if the dropping of z, or equivalently the rising of s, is monotonic on either side of the jump $x = 0$. This factor 2 is to be cancelled out by the existing factor 2 in the denominator, yielding approximately 1, or the counting measure of the jump set $\Gamma = \{0\}$. On the other hand, on could construct a special z that achieves the equality in the last formula, confirming the well approximation of $E_\varepsilon[z]$ to the original geometric measure $E[\Gamma] = \alpha \mathcal{H}^0(\Gamma)$. By using the distance function, the above argument and construction can be naturally extended to the high dimensional case (see Ambrosio and Tortorelli [3, 4]).

Next, one approximates the weberized regularity energy $E_{\mathrm{w}}[u \mid \Gamma]$ using the well function by

$$E_{\mathrm{w}}[u \mid z] = \beta \int_\Omega (z^2 + o_\varepsilon) \frac{|\nabla u|^2}{u^2} dxdy, \tag{6.3}$$

where o_ε stands for any positive scalar parameter that vanishes faster than ε. The role of o_ε is to enforce the uniform ellipticity of the integral even near the edge set Γ where the well function z could be zero or close. Notice that in terms of the logarithmic luminance function $w = \ln u$, one has

$$E_{\rm w}[w \mid z] = \beta \int_\Omega (z^2 + o_\varepsilon)|\nabla w|^2 dxdy, \tag{6.4}$$

Finally recall that the Bose-Einstein noise leads to the generative data model

$$E_{\rm be}[w_0 \mid w] = \lambda \int_\Omega \left(w + e^{w_0 - w}\right) dxdy = \lambda \int_\Omega \psi(w \mid w_0) dxdy, \tag{6.5}$$

where $\psi(t \mid a) = t + \exp(a - t)$ as in the preceding sections.

In combination of (6.1) and (6.4), we propose the Γ-convergence approximation to the weberized Mumford-Shah model with Bose-Einstein noise

$$\begin{aligned} E_{\rm wmsbe}[w, z \mid w_0, \varepsilon] &= E_\varepsilon[z] + E_{\rm w}[w \mid z] + E_{\rm be}[w_0 \mid w] \\ &= \alpha \int_\Omega \left(\varepsilon |\nabla z|^2 + \frac{(z-1)^2}{4\varepsilon}\right) dxdy \\ &\quad + \beta \int_\Omega (z^2 + o_\varepsilon)|\nabla w|^2 dxdy + \lambda \int_\Omega \left(w + e^{w_0 - w}\right) dxdy. \end{aligned} \tag{6.6}$$

Following Ambrosio and Tortorelli's work on the classical Mumford-Shah model, it is possible to establish the existence and convergence theorem, whose proof will be omitted.

THEOREM 6.1. *Assume that $w_0 \in L^\infty(\Omega)$ as in the preceding theorems. Then*

(a) For any fixed $\varepsilon > 0$, the minimizer to $E_{\rm wmsbe}[w, z \mid w_0, \varepsilon]$ exists.

(b) As $\varepsilon \to 0$, the sequence of cost energies $E_{\rm wmsbe}[w, z \mid w_0, \varepsilon]$ converge to $E_{\rm wmsbe}[w, \Gamma \mid w_0]$ in the Γ-convergence sense.

6.2. Euler-Lagrange Equations. To derive the Euler-Lagrange equations associated with (6.6), define the two conditional cost energies as in Section 5. First, for a fixed current estimation of the well function z, one defines the conditional energy

$$E_{\rm wmsbe}[w \mid w_0, \varepsilon, z] = \beta \int_\Omega (z^2 + o_\varepsilon)|\nabla w|^2 dxdy + \lambda \int_\Omega \left(w + e^{w_0 - w}\right) dxdy. \tag{6.7}$$

Variation on w: $w \to w + \delta w$ in $H^1(\Omega)$ leads to the Euler-Lagrange equation

$$0 = -2\beta \nabla \cdot (z^2 + o_\varepsilon)\nabla w + \lambda \left(1 - e^{w_0 - w}\right), \tag{6.8}$$

with Neumann adiabatic conditions $\partial w / \partial \vec{n} = 0$ along $\partial\Omega$. Notice that unlike the Gaussian noise model, the Bose-Einstein noise model makes the Euler-Lagrange equation nonlinear.

For the current best estimation of the logarithmic image w, define the conditional cost energy

$$E_{\rm wmsbe}[z \mid w_0, \varepsilon, w] = \alpha \int_\Omega \left(\varepsilon |\nabla z|^2 + \frac{(z-1)^2}{4\varepsilon}\right) dxdy + \beta \int_\Omega (z^2 + o_\varepsilon)|\nabla w|^2 dxdy. \tag{6.9}$$

Variation on z: $z \to z + \delta z$ in $H^1(\Omega)$ leads to the Euler-Lagrange equation:

$$0 = \alpha \left(-2\varepsilon \Delta z + \frac{z-1}{2\varepsilon} \right) + 2\beta z |\nabla w|^2, \tag{6.10}$$

similarly with Neumann boundary condition. Any minimizer $(w_\varepsilon, z_\varepsilon)$ to $E_{\text{wmsbe}}[w, z \mid w_0, \varepsilon]$ in $H^1(\Omega)$ therefore must satisfy (6.8) and (6.10) in the weak sense.

6.3. An Iterative Algorithm. In this section, we propose an iterative algorithm for solving the system of nonlinear Euler-Lagrange equations just established above.

For a given w, define the linear elliptic operator

$$L_w = -4\varepsilon^2 \Delta + \left(1 + \frac{4\beta\varepsilon}{\alpha} |\nabla w|^2 \right).$$

Then the z-equation (6.10) simply becomes

$$L_w z(x, y) = 1 \qquad (x, y) \in \Omega \tag{6.11}$$

with Neumann boundary condition.

For the w-equation (6.8), define a positive analytic function

$$\phi(t) = \frac{\lambda}{2\beta} \frac{1 - e^{-t}}{t} = \frac{\lambda}{2\beta} \int_0^1 e^{-tp} dp > 0.$$

Then (6.8) becomes

$$0 = -\nabla \cdot (z^2 + o_\varepsilon) \nabla w + (w - w_0) \phi(w - w_0) \tag{6.12}$$

Furthermore, for *given* z and w, define the positive linear elliptic operator

$$M_{z,,w} = -\nabla \cdot (z^2 + o_\varepsilon) \nabla + \phi(w - w_0).$$

Then (6.12) can be written as

$$M_{z,w} w = \phi(w - w_0) w_0, \tag{6.13}$$

which of course becomes nonlinear for w since the operator $M_{z,w}$ itself involves w.

The combination of the structures in (6.11) and (6.13) suggests a natural iterative algorithm. Starting with an initial guess $(w^{(0)}, z^{(0)})$, at step n, $(w^{(n+1)}, z^{(n+1)})$ solves the follow system of linear equations on (w, z):

$$\begin{aligned} M_{z^{(n)}, w^{(n)}} w &= \phi(w^{(n)} - w_0) w_0, \\ L_{w^{(n)}} z &= 1, \end{aligned} \tag{6.14}$$

with Neumann boundary conditions for both w and z. This system of decoupled and linear elliptic equations can be efficiently integrated using any linear elliptic solvers, among which we adopt finite difference based iterative methods.

6.4. Numerical Examples and Comparison with the Mumford-Shah Model.

6.4.1. Γ convergence approximation to the Mumford-Shah model. To make comparison, we also need to establish the Γ-convergence approximation to the ordinary Mumford-Shah model, with either Gaussian noise or Bose-Einstein noise.

In the case of Bose-Einstein noise, the Mumford-Shah model becomes

$$E_{\text{msbe}}[u, \Gamma \mid w_0] = \alpha \mathcal{H}^1(\Gamma) + \beta \int_{\Omega \setminus \Gamma} |\nabla u|^2 dxdy + \lambda \int_\Omega \left(\ln u + \frac{u_0}{u} \right) dxdy,$$

whose Γ-convergence approximation could similarly be established:

$$\begin{aligned} E_{\text{msbe}}[u, z \mid u_0, \varepsilon] = \alpha \int_\Omega \left(\varepsilon |\nabla z|^2 + \frac{(z-1)^2}{4\varepsilon} \right) dxdy \\ + \beta \int_\Omega (z^2 + o_\varepsilon) |\nabla u|^2 dxdy + \lambda \int_\Omega \left(\ln u + \frac{u_0}{u} \right) dxdy, \end{aligned} \tag{6.15}$$

Similar to the preceding section, one obtains the Euler-Lagrange equations:

$$\begin{aligned} 0 &= -2\beta \nabla \cdot (z^2 + o_\varepsilon) \nabla u + \frac{\lambda}{u^2}(u - u_0), \\ 0 &= \alpha \left(-2\varepsilon \Delta z + \frac{z-1}{2\varepsilon} \right) + 2\beta |\nabla u|^2 \, z, \end{aligned} \tag{6.16}$$

with Neumann adiabatic boundary conditions. Notice that without weberization, the equations are naturally about (u, z) instead of $(w = \ln u, z)$, as in contrast with Eqn. (6.8) and (6.10).

This system of nonlinear elliptic equations can be similarly integrated by iterations based on stepwise linearization. That is, at each step n, $(u^{(n+1)}, z^{(n+1)})$ solves the follow system on (u, z):

$$\begin{aligned} 0 &= -2\beta \nabla \cdot ([z^{(n)}]^2 + o_\varepsilon) \nabla u + \frac{\lambda}{[u^{(n)}]^2}(u - u_0), \\ 0 &= \alpha \left(-2\varepsilon \Delta z + \frac{z-1}{2\varepsilon} \right) + 2\beta |\nabla u^{(n)}|^2 \, z. \end{aligned} \tag{6.17}$$

As before, o_ε denotes any scalar sequence that vanishes faster than ε as $\varepsilon \to 0^+$.

These are the equations to be solved for comparison with their weberized versions in (6.14).

In the case of Gaussian noises, the system of equations (6.16) and (6.17) still hold after the removal of u^2 or $[u^{(n)}]^2$ in the denominators associated with the fitting terms, which is of course a coupled linear system.

6.4.2. Strength of edges based on Γ-convergence approximation. Γ-convergence approximation also provides a natural way to define the *strength* of an optimal edge well function z_ε, which can be a useful measure in evaluating and comparing the performances of different models. To the best knowledge of the authors, we are the first to endow the edge well or wall function with such meaning.

We define the edge *strength* at bandwidth ε by

$$\hat{\eta}_\varepsilon = \int_\Omega |\nabla s_\varepsilon(x, y)| dxdy = \text{TV}(s_\varepsilon),$$

i.e., the total variation of the "wall" function $s_\varepsilon = (1 - z_\varepsilon)^2$. This has been primarily motivated by the analysis in the beginning of Section 6.1, in particular, the Schwarz inequality (6.2), as well as the construction technique in the proof by Ambrosio and Tortorelli [4].

For the optimal wall function s_ε, denote its height by $d_\varepsilon \in [0, 1]$. Then the edge strength is approximately given by

$$\hat{\eta}_\varepsilon = \mathrm{TV}(s_\varepsilon) \simeq 2d_\varepsilon \ \mathrm{length}(\Gamma), \tag{6.18}$$

which justifies $\hat{\eta}_\varepsilon$ as a measure of edge strength - larger d_ε values correspond to stronger edges. Here the factor 2 comes from the two sides of the "wall." Approximation (6.18) at least holds locally along any stationary (i.e., with almost constant height) segment of the walls, and can be further justified by the celebrated co-area formula of De Giorgi [23], and Fleming and Rishel [19] on the total variation Radon measure (also see [12, 23]):

$$\mathrm{TV}(s_\varepsilon) = \int_\Omega |Ds_\varepsilon| = \int_0^1 \mathrm{length}(s_\varepsilon \equiv \lambda) d\lambda, \qquad (\textit{the co-area formula})$$

where $(s_\varepsilon \equiv \lambda)$ denotes the λ-level set of s_ε. For simplicity, s_ε has been assumed to be smooth, otherwise, the length measure should be replaced by the *perimeter* of the cumulative level sets $\{s_\varepsilon > \lambda\}$. Therefore, if the wall is steep in the transition from the ground value s_- to the peak value s_+, as should be in the case of small ε, each level set $s_\varepsilon \equiv \lambda$ consists of two slightly translated copies of the edge curve Γ on either side of the wall. As a result,

$$\mathrm{TV}(s_\varepsilon) \simeq \int_{s_-}^{s_+} 2\mathrm{length}(\Gamma) d\lambda = 2(s_+ - s_-)\ \mathrm{length}(\Gamma),$$

which is precisely (6.18).

Practically, or at least locally along a stationary edge segment, it is also convenient to simply consider the *relative* strength

$$\eta_\varepsilon := \max_{(x,y)\in\Omega} z_\varepsilon(x, y) - \min_{(x,y)\in\Omega} z_\varepsilon(x, y),$$

which is proportional to $d_\varepsilon = s_+ - s_-$ just defined above. It could be considered as the absolute strength $\hat{\eta}_\varepsilon$ modulated by the length of the underlying segment according to (6.18), and can be useful in comparing the relative edge strengthes output from different models (e.g., Figure 6.1 and 6.2). Visually, one simply inspects the darkness of the well functions along the targeted edges, since their maximal values are always close to 1 for small ε (as guaranteed by the term $(z - 1)^2/(4\varepsilon)$ in the Γ-convergence approximations). Thus, darker edges are stronger.

6.4.3. Two examples and comparisons. We illustrate the performance of our new model through two image examples: one synthetic and the other an image of a real 3-dimensional scene designed by the first author.

The synthetic image example in Figure 6.1 is to verify and highlight the light adaptivity of our new model, while the real image in Figure 6.2 is to compare the performances of our new model with the classical Mumford-Shah model (6.16) and (6.17) in terms of light adaptivity.

Both figures have been generated by Matlab codes, which implement the two algorithms (6.14) and (6.17). The Matlab codes for the several files involved, as well as the real image designed by the first author (in Figure 6.2), are available under request.

Both noises have been simulated by using Matlab's random number generators, and Figure 6.1 involves simulated Gaussian noise while Figure 6.2 simulated Bose-Einstein noise. Notice that the least square fitting energy is employed in both models in the case of Gaussian noise.

Since it is better to read the interpretation of the computational results while staring at the figures, our comments, views, and explanations are detailed directly in the captions of the two figures.

From these examples, we conclude that

(a) The *weberized* Mumford-Shah model indeed faithfully embodies Weber's Law, and demonstrates clear light adaptivity parallel to the way that human vision functions.

(b) Due to the gray-scale shift invariance, the classical Mumford-Shah model does not faithfully simulate light adaptivity of human visual perception as predicted by both Weber's Law and retinal physiology [27, 18, 53, 50].

7. Conclusion. Towards a more faithful model of human visual segmentation, the current paper introduces the light adaptivity feature into the celebrated Mumford-Shah segmentation model [38], as inspired by Weber's Law in both vision psychology and retinal physiology [17, 18, 35, 39, 42, 45, 49, 50, 53]. To be consistent with the intensity (or photon counting) interpretation of images in the weberization procedure, the traditional gray scale shift-invariant Gaussian noise model is accordingly replaced by Bose-Einstein photon noise.

Among the very few first works on this new direction, the current paper gives a detailed account of Weber's Law in terms of both vision psychology and retinal physiology. The rationale behind the weberization of the classical Mumford-Shah model is also carefully explained.

Both theoretical analysis and computational algorithms are developed for the weberized Mumford-Shah model with Bose-Einstein noise. In particular, Ambrosio and Tortorelli's Γ-convergence approximation procedure has been adapted to the new model, and the resulting system of nonlinear Euler-Lagrange equations are numerically integrated by a stable iterative algorithm based on a linearization technique.

Computational results have convincingly confirmed the light adaptivity feature of the new model. Comparison with the classical Mumford-Shah model further highlights the noticeable improvement achieved by the new model.

Unlike many other previous works of the first author, the current work is more oriented toward

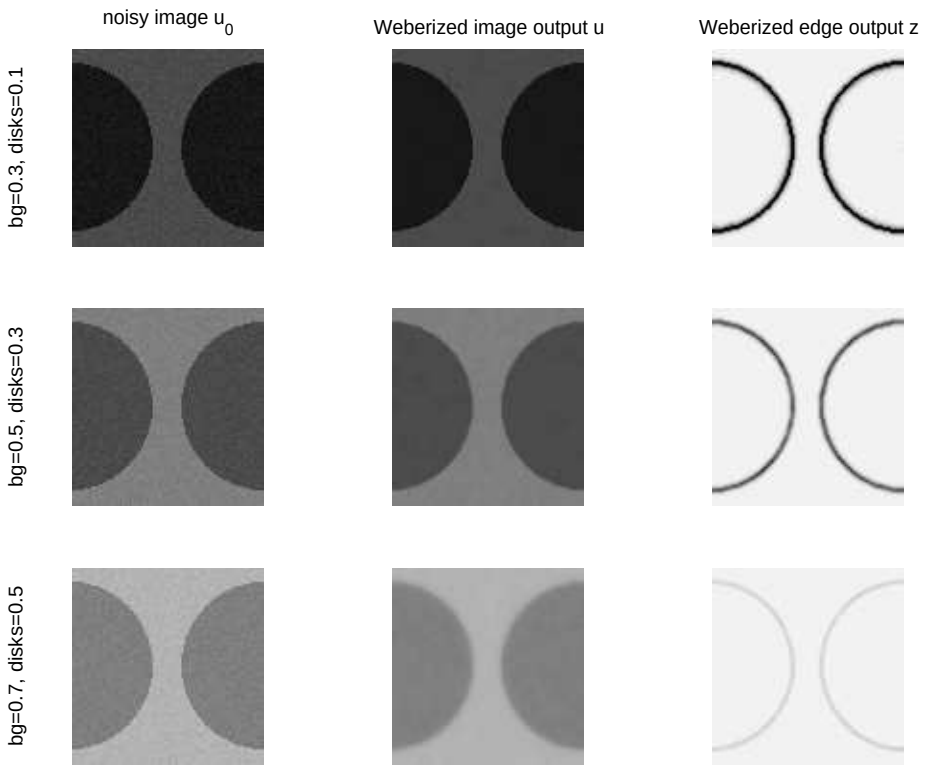

FIG. 6.1. *Performance via a synthetic image: light adaptivity of the weberized Mumford-Shah model (in the setting of* Γ*-convergence approximation). Each noisy image is obtained from the immediately above by a simple intensity increment of* 0.2 *everywhere in the scale of [0,1]. By the weberized Mumford-Shah model, as consistent with Weber's Law, the edge functions* z *are distinct and have relative strengthes* $\eta_\varepsilon = \max z_\varepsilon - \min z_\varepsilon = 0.98, 0.75, 0.20$ *separately. The classical Mumford-Shah model is contrast shift-invariant (see Theorem 1.1), and therefore makes no distinction among the three, which is less faithful in vision modelling according to the real perceptual responses characterized by Weber's Law. All three examples are computed using a same set of visual potentials* (α, β, λ) *as well as the* Γ*-convergence bandwidth* ε.

faithful modelling of the *real* human vision system, instead of strongly driven by the necessity of digital image processing, although the two are intimately connected. The current work therefore should be best judged by its value in exemplifying and promoting more faithful models in vision research by integrating important experimental as well as theoretical results in psychology, physiology and biology, and the very nature of light and photons offered by quantum and statistical mechanics.

Acknowledgments. The first author would like to thank Professors Gilbert Strang, Tony Chan, David Mumford, Jayant Shah, Song-Chun Zhu, Dan Kersten, James Keener, Hans Othmer, Steve Smale, Bob Gulliver, and Antonin Chambolle for their invaluable teaching and inspirations, as well as the Applied Mathematics Program of NSF (USA) under the grant number DMS-0202565 for her generous support. The authors also acknowledge the profound benefits received from the Institute

of Mathematics and its Applications (IMA, funded by USA-NSF) at the University of Minnesota, where James Keener and his colleagues gave very encouraging tutorials on mathematical biology and physiology in the summer of 2003. The first author would also like to acknowledge the warm support and numerous inspirations from the conference on neuron modelling and computation celebrating the 60th birthday of Nancy Kopell at the Boston University in the April of 2003. The current project would have become impossible without the initial random bumping of all the ideas nourished by the aforementioned inspirations.

REFERENCES

[1] G. Alberti and C. Mantegazza. A note on the theory of SBV functions. *Bollettino U. M. I.*, 7(11-B):375–382, 1997.

[2] L. Ambrosio. A compactness theorem for a new class of functions of bounded variation. *Bollettino U. M. I.*, 7(3-B):857–881, 1989.

[3] L. Ambrosio and V. M. Tortorelli. Approximation of functionals depending on jumps by elliptic functionals via Γ-convergence. *Comm. Pure Appl. Math.*, 43:999–1036, 1990.

[4] L. Ambrosio and V. M. Tortorelli. On the approximation of free discontinuity problems. *Boll. Un. Mat. Ital.*, 6-B:105–123, 1992.

[5] C. M. Bender and S. A. Orszag. *Advanced Mathematical Methods for Scientists and Engineers.* McGrawHill, Inc., 1978.

[6] F. Catté, P.-L. Lions, J.-M. Morel, and T. Coll. Image selective smoothing and edge detection by nonlinear diffusion. *SIAM J. Numer. Anal.*, 29:182–193, 1992.

[7] A. Chambolle. Image segmentation by variational methods: Mumford and Shah functional and the discrete approximations. *SIAM J. Appl. Math.*, 55(3):827–863, 1995.

[8] A. Chambolle. Finite-differences discretizations of the Mumford-Shah functional. *M2AN Math. Model. Numer. Anal.*, 33(2):261–288, 1999.

[9] A. Chambolle and P. L. Lions. Image recovery via Total Variational minimization and related problems. *Numer. Math.*, 76:167–188, 1997.

[10] T. F. Chan, S.-H. Kang, and J. Shen. Euler's elastica and curvature based inpaintings. *SIAM J. Appl. Math.*, 63(2):564–592, 2002.

[11] T. F. Chan and J. Shen. Mathematical models for local nontexture inpaintings. *SIAM J. Appl. Math.*, 62(3):1019–1043, 2001.

[12] T. F. Chan and J. Shen. On the role of the BV image model in image restoration. *Amer. Math. Soc. Contemporary Mathematics,* volume 330 on *Recent Advances in Scientific Computing and Partial Differential Equations,* Editors: S. Y. Cheng, C.-W. Shu, and T. Tang, pages 25–41, 2003.

[13] T. F. Chan, J. Shen, and L. Vese. Variational PDE models in image processing. *Amer. Math. Soc. Notice*, 50:14–26, 2003.

[14] T. F. Chan and L. Vese. A level set algorithm for minimizing the Mumford-Shah functional in image processing. *IEEE/Computer Society Proceedings of the 1st IEEE Workshop on "Variational and Level Set Methods in Computer Vision"*, pages 161–168, 2001.

[15] D. Chandler. *Introduction to Modern Statistical Mechanics.* Oxford University Press, New York and Oxford, 1987.

[16] S. Esedoglu and J. Shen. Digital inpainting based on the Mumford-Shah-Euler image model. *European J. Appl. Math.*, 13:353–370, 2002.

[17] G. Fain and Matthews H. R. Calcium and the mechanism of light adaptation in vertebrate photoreceptors. *Trends*

Neurosci., 13:378–384, 1990.

[18] G. T. Fechner. Über ein wichtiges psychophysiches Grundgesetz und dessen Beziehung zur Schäzung der Sterngrössen. Abk. k. Ges. Wissensch. *Math.-Phys.*, K1, 4, 1858.

[19] W. H. Fleming and R. Rishel. An integral formula for total gradient variation. *Arch. Math.*, 11:218–222, 1960.

[20] S. Geman and D. Geman. Stochastic relaxation, Gibbs distributions, and the Bayesian restoration of images. *IEEE Trans. Pattern Anal. Machine Intell.*, 6:721–741, 1984.

[21] W. Gibbs. *Elementary Principles of Statistical Mechanics.* Yale University Press, 1902.

[22] E. De Giorgi, M. Carriero, and A. Leaci. Existence theorem for a minimization problem with free discontinuity set. *Arch. Rational Mech. Anal.*, 108:195–218, 1989.

[23] E. Giusti. *Minimal Surfaces and Functions of Bounded Variation.* Birkhäuser, Boston, 1984.

[24] U. Grenander. *Lectures in Pattern Theory. I. II. and III.* Springer, 1976-1981.

[25] D. H. Hubel and T. N. Wiesel. Receptive fields, binocular intersection and functional architecture in the cat's visual cortex. *Journal of Physiology*, 160:106–154, 1962.

[26] M. Kass, A. Witkin, and D. Terzopoulos. Snakes: active contour models. *ICCV 1987*, 777, 1987.

[27] J. Keener and J. Sneyd. *Mathematical Physiology.* Interdisciplinary Applied Mathematics. Springer, New York, 1998.

[28] E. H. Lieb and M. Loss. *Analysis.* Amer. Math. Soc., second edition, 2001.

[29] R. March. Visual reconstruction with discontinuities using variational methods. *Image Vision Comput.*, 10:30–38, 1992.

[30] R. March and M. Dozio. A variational method for the recovery of smooth boundaries. *Image Vision Comput.*, 15:705–712, 1997.

[31] D. Marr. *Vision.* Freeman, San Francisco, 1980.

[32] D. Marr and E. Hildreth. Theory of edge detection. *Proc. Royal Soc. London*, B:207: 187–217, 1980.

[33] J. T. Marti. *Introduction to Sobolev Spaces and Finite Element SolutionElliptic Boundary Value Problems.* Academic Press, 1986.

[34] G. Dal Maso, J.-M. Morel, and S. Solimini. A variational method in image segmentation: Existence and approximation results. *Acta. Math.*, 168:89–151, 1992.

[35] P. A. McNaughton. Light response of vertebrate photoreceptors. *Physiological Reviews*, 70:847–883, 1990.

[36] J. W. Milnor. *Topology from the Differentiable Viewpoint.* Princeton Univ. Press, revised edition, 1997.

[37] D. Mumford. *Geometry Driven Diffusion in Computer Vision*, chapter "The Bayesian rationale for energy functionals", pages 141–153. Kluwer Academic, 1994.

[38] D. Mumford and J. Shah. Optimal approximations by piecewise smooth functions and associated variational problems. *Comm. Pure Applied. Math.*, 42:577–685, 1989.

[39] R. A. Norman and I. Perlman. The effects of background illumination on the photoresponses of red and green cones. *J. Physiology*, 286:491–507, 1979.

[40] S. Osher and J. A. Sethian. Fronts propagating with curvature-dependent speed: Algorithms based on Hamilton-Jacobi formulations. *J. Comput. Phys.*, 79(12), 1988.

[41] T. Poggio and S. Smale. The mathematics of learning: Dealing with data. *Amer. Math. Soc. Notice*, 50(5):537–544, 2003.

[42] E. N. Pugh and T. D. Lamb. Cyclic GMP and calcium: messengers of excitation and adaptation in vertebrate photoreceptors. *Vision Research*, 30:1923–1948, 1990.

[43] L. Rudin and S. Osher. Total variation based image restoration with free local constraints. *Proc. 1st IEEE ICIP*, 1:31–35, 1994.

[44] L. Rudin, S. Osher, and E. Fatemi. Nonlinear total variation based noise removal algorithms. *Physica D*, 60:259–268, 1992.

[45] R. M. Shapley and C. Enroth-Cugell. Visual adaptation and retinal gain controls. In: *Progress in Retinal Research,* Ed: N. Osborne and G. Chader; Pergamon Press, London, 1984.

[46] J. Shen. Inpainting and the fundamental problem of image processing. *SIAM News*, 36(2), 2003.

[47] J. Shen. On the foundations of vision modeling I. Weber's law and Weberized TV restoration. *Physica D*, 175:241–251, 2003.

[48] A. N. Tikhonov. Regularization of incorrectly posed problems. *Soviet Math. Dokl.*, 4:1624–1627, 1963.

[49] D. Tranchina, J. Gordon, and R. Shapley. Retinal light adaptation - evidence for a feedback mechanism. *Nature*, 310:314–316, 1984.

[50] D. Tranchina and C. S. Peskin. Light adaptation in the turtle retina: embedding a parametric family of linear models in a single nonlinear model. *Visual Neuroscience*, 1:339–348, 1988.

[51] A. Tsai, Jr. A. Yezzi, and A. S. Willsky. Curve evolution implementation of the Mumford-Shah functional for image segmentation, denoising, interpolation and magnification. *IEEE Trans. Image Process.*, 10(8):1169–1186, 2001.

[52] C. Vogel. *Computational Methods for Inverse Problems.* SIAM, Philadelphia, 2002.

[53] E. H. Weber. De pulsu, resorptione, audita et tactu. *Annotationes anatomicae et physiologicae,* Leipzig: Koehler, 1834.

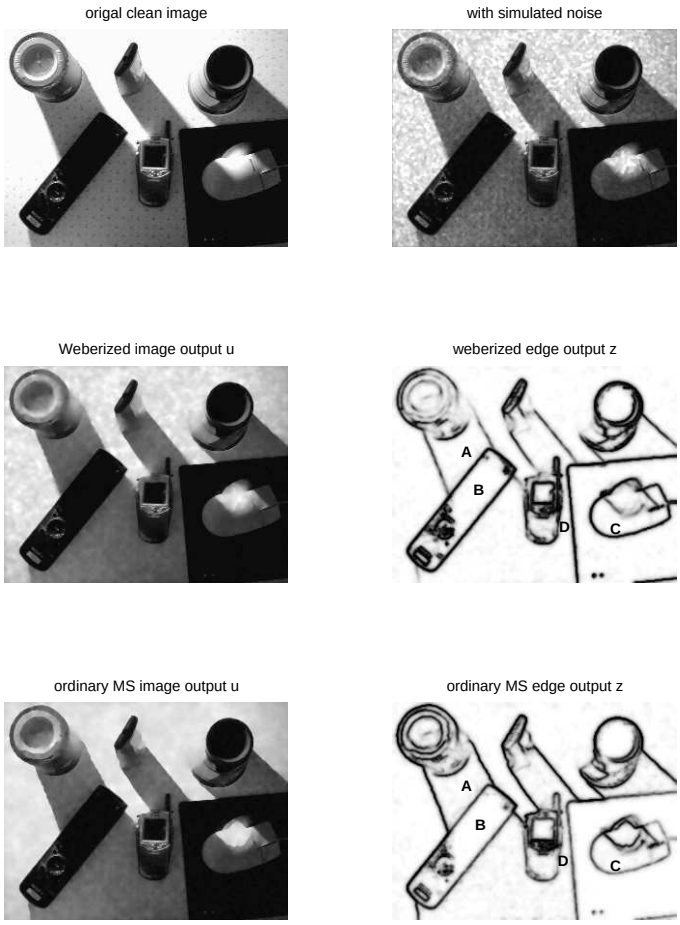

FIG. 6.2. *Performance comparison via a real image between the ordinary Mumford-Shah model and its weberization (in the setting of* Γ*-convergence approximation with a same bandwidth parameter* ε*). The scene setting and illuminance direction in the original picture have been designed by the first author to create an image with a large dynamic range of intensity values. In particular, the shadows have been intentionally introduced to create dimmer regions. Notice that for objects in the shadows (i.e., the control panel* $\boldsymbol{B}$*, cell phone* $\boldsymbol{D}$*, and the mouse and mouse pad* $\boldsymbol{C}$*), the edges detected are still strong in the weberized Mumford-Shah model while get weaker in the ordinary Mumford-Shah model. That is, along the edges in the shadows, the relative strengthes* η_ε *are much stronger from the weberized model than the original one. On the other hand, the boundaries of the shadows themselves (e.g., shadow A of the pen holder) against a brighter background are stronger in the Mumford-Shah model than its weberization. From the* constancy *of the edge strengthes of the control panel (B) or the mouse (C), it is clear that the weberized model is insensitive to external illuminance conditions, and captures the edges of the objects equally well whether they are under direct illumination or in the shadows, which well resonates with Shapley and Enroth-Cugell's remarkable inference in Theorem 2.3. All these results are consistent with the light adapted capability of human visual perception, as predicted by Weber's Law.*